Nanopatterned Polymer Brushes for Triggered Detachment of Anchorage-Dependent Cells

*Qian Yu, Leah M. Johnson, and Gabriel P. López**

Surfaces modified with thermoresponsive poly(*N*-isopropylacrylamide) (PNIPAAm) support mild and efficient harvesting of anchorage-dependent cells. To enable cellular detachment, however, the surfaces must exhibit a narrow range of PNIPAAm thicknesses. In this work, this limitation is circumvented by introducing nanopatterns to grafted PNIPAAm brushes, eliminating the critical thickness requirement for cell-culturing applications. Nanopatterned PNIPAAm surfaces are prepared using a combination of interferometric lithography (IL) and surface-initiated polymerization. Above the lower critical solution temperature (LCST) of PNIPAAm (~32 °C), these surfaces support the attachment and proliferation of mammalian cells (e.g., fibroblasts and endothelial cells). Below the LCST of PNIPAAm, cells readily detach from the nanopatterned PNIPAAm surfaces without influence from the period of nanopatterns, which vary between 157 ± 9 nm to 1021 ± 17 nm. Cells selectively attach and proliferate on PNIPAAm nanopatterns as compared to thick unpatterned PNIPAAm, which is further exploited to spatially direct cellular growth to generate cellular micropatterns. Nanopatterned PNIPAAm surfaces provide a unique solution to the critical thickness issue for cell harvesting and facilitate spatial control of cellular growth on surfaces.

1. Introduction

The ability to recover anchorage dependent cells from substrates is crucial for a variety of purposes including cell-based regenerative therapy, tissue engineering, and fundamental biological studies.[1–3] Conventional methods for harvesting mammalian cells from substrates involve either enzymatic or mechanical processes.[4,5] One prominent harvesting method uses proteases, such as trypsin or dispase, to enzymatically release cells from the underlying substrate. Alternatively, mechanical dissociation via cell scraping is often used with cell lines that are sensitive to the proteolytic digestion protocol. Although serving as the mainstay of standard tissue culture, these harvesting methods often jeopardize cellular integrity by affecting the extracellular matrix (ECM) and membrane proteins. Moreover, these traditional harvesting methods may subject cells to unnecessary stresses undesirable for cell biology applications. The fundamental research and accompanying applications involving mammalian cell culture would greatly benefit from an easy and mild alternative approach for cell harvesting.

One alternative method for cell harvesting employs substrates modified with the thermo-responsive polymer, poly(*N*-isopropylacrylamide) (PNIPAAm).[6,7] PNIPAAm has been well studied in biological applications, owing to its responsiveness in aqueous solutions near physiological temperature ranges. Specifically, below its lower critical solution temperature (LCST) of 32 °C, PNIPAAm chains hydrate and swell into extended conformations in water.[8] Conversely, above its LCST, PNIPAAm chains collapse into less hydrated and condensed morphological arrangements, which exhibit relatively hydrophobic characteristics.[9–11] Because of this property, PNIPAAm modified surfaces can be used to dynamically control surface properties such as wettability and bioadhesion.[12–14] For example, pioneering work by Okano et al. exploited PNIPAAm modified surfaces to harvest intact cell sheets in a mild and facile manner.[15] At 37 °C, in the presence of adsorbed ECM proteins, cells attach to and proliferate on PNIPAAm surfaces, similar to their behavior on standard tissue culture polystyrene dishes. However, at temperatures below the LCST of PNIPAAm (e.g., 20 °C), the cells readily detach from the surface, likely due to the hydration and change in morphology of hydrophilic PNIPAAm chains. The mild disruption between the cells and the PNIPAAm modified surfaces preserves cellular integrity more easily than traditional harvesting methods.[3]

Although using PNIPAAm for cellular harvesting is effective, the attachment and detachment of cells depends critically on the thickness of the (unpatterned) PNIPAAm brushes or films.[16–19] Specifically, PNIPAAm layers must exhibit a narrow range of thickness (or molecular weight) to support cellular attachment to, *and* subsequent detachment from, the thermoresponsive substrate surface. If the thickness of PNIPAAm is less than a minimum critical dimension, cells readily attach to the surface, but will not detach at temperatures below the

Dr. Q. Yu, Dr. L. M. Johnson, Prof. G. P. López
Department of Biomedical Engineering
Duke University
Durham NC, 27708, USA
E-mail: gabriel.lopez@duke.edu
Prof. G. P. López
Department of Mechanical Engineering and Materials Science
Duke University, Durham, NC, 27708, USA
NSF Research Triangle Materials Research Science & Engineering Center
Duke University
Durham, NC 27708, USA

DOI: 10.1002/adfm.201304274

LCST. Conversely, if the PNIPAAm layer is thicker than a maximum critical dimension, cells cannot attach to the surface, regardless of the temperature.[17] Considerable research efforts have focused on solving this "thickness" dilemma. For example, strategies to encourage cell attachment on thicker PNIPAAm include copolymerization with a hydrophobic monomer[20] or covalent immobilization of cell-adhesive biomolecules.[21,22] Likewise, to encourage release of cells from thinner PNIPAAm, porous membranes,[23] comb-like polymer architectures,[24] and hydrophilic segments,[25,26] have been used.

In general, cells respond not only to surface chemistries, but also to surface topologies. For instance, cell-surface interactions are greatly influenced by nanotopography and nanoscale roughness of synthetic surfaces.[27,28] We reasoned that combining the thermo-responsive characteristic of PNIPAAm with a well-defined nanopatterned features would result in a unique capacity for cellular harvesting. We have previously used nanopatterned PNIPAAm brushes to modulate bioactivity on surfaces by dynamically controlling the display of biomolecules immobilized on polymer-free regions between the brushes.[29,30] Our studies showed that nanopatterned PNIPAAm chains collapse and can expose biomolecules at temperatures above the LCST, while PNIPAAm chains swell and can hide bioactive moieties at temperatures below the LCST. This transition between biologically 'active' and 'inactive' states encouraged our further investigation into using nanopatterned PNIPAAm for harvesting of adherent mammalian cells. We reasoned that cells would respond to ECM molecules immobilized in the polymer-free regions, thereby negating the need to maintain a critical thickness and facilitating control of cell attachment and detachment.

In this work, we show that the introduction of nanopatterns into PNIPAAm brushes results in unique benefits for cellular detachment and harvesting. Our findings reveal that the presence of nanopatterns alleviates the requirement to maintain a narrow range of brush thickness for harvesting of fibroblasts and endothelial cells from PNIPAAm brushes. We detail the effects of polymerization time and period size on cellular attachment and detachment. We anticipate that incorporating nanopatterns within thermo-responsive polymers will benefit applications involving cellular micropatterning, cell harvesting, and cell sheet engineering.

2. Results and Discussion

2.1. Preparation and Characterization of Nanopatterned PNIPAAm Surfaces

The fabrication of surfaces with nanopatterned PNIPAAm brushes involved a combination of "top-down" and "bottom up" strategies (**Scheme 1**).[29] Surfaces were prepared via a combination of interference lithography (IL) and surface-initiated, activator regenerated by electron transfer-atom transfer radical polymerization (ARGET-ATRP), which enables precise control of surface properties.[31,32] First, we regio-selectively photodegraded self-assembled monolayers (SAMs) of ATRP initiator using UV-IL. IL is a simple method capable of forming periodic-patterns of nanoscale over large surface areas.[33] We then used surface-initiated polymerization (SIP) to graft PNIPAAm brushes from these nanopatterned initiators via ARGET-ATRP. The chain length of grafted PNIPAAm brushes was adjusted by changing the polymerization time,[32] whereas the spatial period of the resultant nanopatterned PNIPAAm surfaces was adjusted by changing the interference angle.[30] **Figure 1** shows the atomic force microscopy (AFM) height images and the corresponding line profiles (cross sections) of four nanopatterned PNIPAAm surfaces with different periods. The peak-to-valley distance (PVD) of the AFM images increased from 7.5 ± 1.2 nm to 59.6 ± 2.3 nm as the pattern period increased from 157 ± 9 nm to 1021 ± 17 nm. This correlation between the PVDs and pattern period suggests that the height of nanopatterned polymer brushes increases as the lateral width of the brush area increases, consistent with previous computer simulations[34] and experimental results.[35] Moreover, the measured PVD values of all nanopatterned PNIPAAm brushes are less than the thickness of corresponding unpatterned PNIPAAm brushes (78.8 ± 3.5 nm, see below). This may be attributed to the lower surface density of initiator molecules in the nanopatterned areas[36] and/or the lateral extension of polymer chains to adjacent non-grafted substrates.[37,38]

We prepared unpatterned PNIPAAm surfaces under various polymerization times and measured the corresponding thickness ($t_{PNIPAAm}$) in air using ellipsometry. Under the experimental conditions explored, we found an approximately linear increase in thickness of the grafted layer (from 13.0 ± 1.7 nm to 78.8 ± 3.5 nm) with increasing polymerization time (from

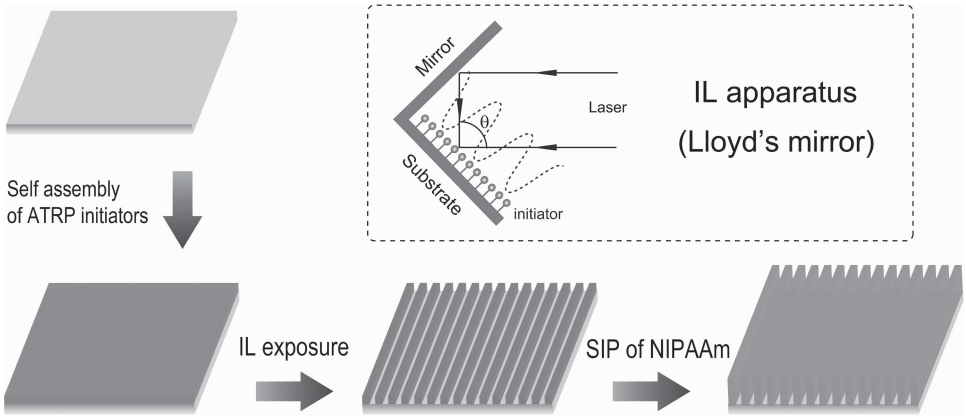

Scheme 1. Steps used in the preparation of nanopatterned PNIPAAm surfaces.

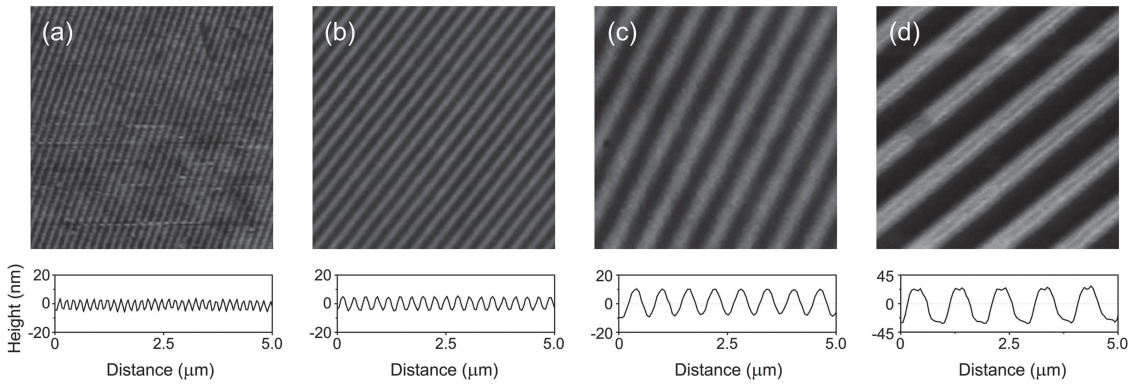

Figure 1. Contact-mode AFM height images obtained in air of nanopatterned PNIPAAm surfaces generated at a constant polymerization time (6 min, corresponding to $t_{PNIPAAm}$ = 78.8 ± 3.5 nm) and different periods: (a) period = 157 ± 9 nm; (b) period = 274 ± 14 nm; (c) period = 625 ± 15 nm; (d) period = 1021 ± 17 nm. The representative cross sections (line profiles) are shown below the AFM images. The field of view is 5 × 5 μm^2 in all images.

1 to 6 min; SI, Figure S1). Please note that, when we refer to nanopatterned surfaces, the term $t_{PNIPAAm}$ denotes the thickness of unpatterned PNIPAAm brush that results for the same polymerization time. We also measured captive bubble contact angle (θ) of nanopatterned PNIPAAm surfaces in water at 25 °C and at 45 °C (i.e., ~10 °C above and below 32 °C, the nominal LCST for PNIPAAm in pure water; SI, Figure S2). The difference of contact angle ($\Delta\theta$) is 14.6 ± 1.5° (from 26.1 ± 1.5° to 40.6 ± 3.5° at 25 °C and at 45 °C, respectively), which is comparable with 16.8 ± 2.1° (from 25.1 ± 1.0° to 42.1 ± 2.5°) for the unpatterned PNIPAAm surfaces, indicating that the introduction of nanopatterned features did not significantly alter the thermal-responsive wettability of PNIPAAm grafted surfaces.

2.2. Adsorption of Fibronectin on Nanopatterned PNIPAAm Surfaces

Fibronectin (FN), a component of the ECM, is commonly adsorbed on synthetic surfaces to support cellular attachment and growth.[39,40] Based on our previous findings,[29] we expected FN to selectively adsorb on polymer-free intervals between nanopatterned PNIPAAm at temperatures above the LCST. We hypothesized that the pre-adsorption of FN on the underlying substrate would facilitate the attachment and growth of cells on nanopatterned PNIPAAm brushes. To evaluate the adsorption of FN on PNIPAAm nanopatterned surfaces, samples were prepared that contained both micropatterns and nanopatterns on the same sample.[29] The surface preparation, as further detailed in Scheme S1a, resulted in micron-sized square areas with unpatterned, photodegraded initiator and striped areas with nanopatterned PNIPAAm. After incubation with a fluorescent FN (i.e., rhodamine-FN) at different temperatures, 25 °C or 37 °C, the fluorescent intensities of the nanopatterned and the unpatterned areas on the same sample were directly compared (**Figure 2**).

The fluorescence images in Figure 2a,b show demarcation between areas containing nanopatterned PNIPAAm brushes (darker stripes) and unpatterned areas with degraded initiators (no PNIPAAm, brighter squares). Because nanoscale features

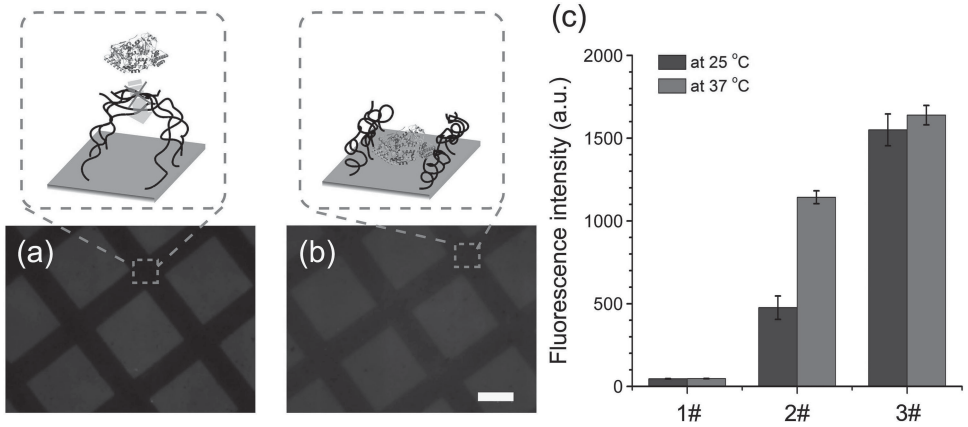

Figure 2. (a,b) Fluorescence images showing surfaces with micro and nanopatterns (period = 274 ± 14 nm and with corresponding $t_{PNIPAAm}$ = 78.8 ± 3.5 nm) after adsorption with rhodamine-FN (0.01 mg/mL in PBS) for 4 h at (a) 25 °C and (b) 37 °C, respectively. (c) Corresponding fluorescence intensities; error bars represent the standard deviation of the mean (n = 10, *** $p < 0.001$). Fluorescence intensity values were acquired from surface locales containing degraded initiator (bright squares in a,b), nanopatterned PNIPAAm (dark lines in a,b) or unpatterned PNIPAAm surfaces with a thickness of 78.8 ± 3.5 nm (not shown pictorially here).

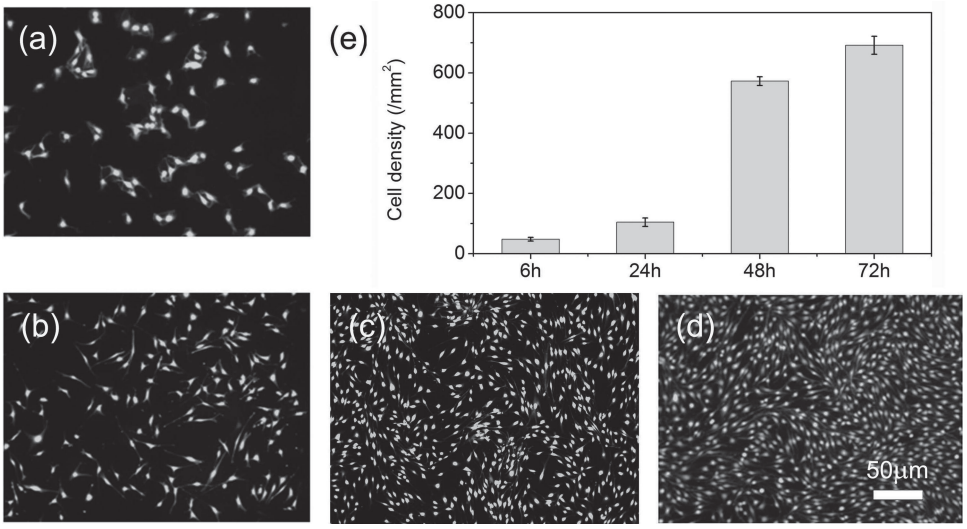

Figure 3. Representative images of NIH-3T3 fibroblasts on a nanopatterned PNIPAAm/FN surface (period = 274 ± 14 nm, $t_{PNIPAAm}$ = 78.8 ± 3.5 nm) after different culturing times at 37 °C for (a) 6 h; (b) 24 h; (c) 48 h; and (d) 72 h. The corresponding number of attached cells is shown in (e); error bars represent the standard deviation of the mean (n = 10).

exist below the resolution of optical microscopy, areas containing nanopatterned PNIPAAm appear as stripes resulting from the pattern of the microscale mask used during the preparation of the micropatterned surfaces. The accompanying fluorescence intensities of surfaces incubated with rhodamine-FN at 25 °C and 37 °C were quantified and are summarized in Figure 2c. The extent of FN adsorption on areas with nanopatterned PNIPAAm was dictated by the temperature used during adsorption of FN. For example, FN strongly adsorbed to nanopatterned PNIPAAm at a temperature above the LCST (37 °C, 1,142 ± 38 a.u) as compared to a temperature below the LCST (25 °C, 475 ± 70 a.u.). FN strongly adsorbed to areas containing degraded initiator (brighter squares) irrespective of temperature, consistent with previous reports.[29] Conversely, FN minimally adsorbed to unpatterned PNIPAAm surfaces, reflecting the protein-resistant properties of PNIPAAm brushes.[41]

The insets in Figure 2a,b illustrate schematically our understanding of this thermally responsive adsorption behavior. At 25 °C, PNIPAAm chains adopt an extended conformation and spread laterally to cover the adjacent substrate and block access of FN to the substrate. At 37 °C, the PNIPAAm chains collapse and retract to expose the substrate and facilitate the adsorption of FN onto the polymer-free intervals. Taken together, these data support the concept that conformational changes of PNIPAAm brushes enable a dynamic exposure and shielding of the polymer-free intervals to support adsorption of FN in a temperature-responsive manner.

2.3. Attachment and Detachment of Mammalian Cells on Nanopatterned PNIPAAm/FN Surfaces

Several research groups have used unpatterned PNIPAAm surfaces to support the culture and harvesting of anchorage dependent cells.[3–5,16–20] However, a surface must exhibit a narrow defined range of thickness of the unpatterned PNIPAAm to support *both* cellular attachment (at T > LCST) and detachment (at T < LCST).[17] If PNIPAAm layer is too thick, then cells do not attach and proliferate; if PNIPAAm layer is too thin, then cells attach but do not detach at T < LCST. Here, we confirmed these trends for unpatterned PNIPAAm surfaces that had been pre-exposed to FN. Cells failed to attach to thicker unpatterned brushes (e.g., $t_{PNIPAAm}$ = 78.8 ± 3.5 nm), but readily attached to, and proliferated on, thinner unpatterned brushes (e.g., $t_{PNIPAAm}$ = 8.2 ± 1.1 nm), unmodified glass substrates and surfaces containing degraded initiator (SI, Figures S3,S4). As expected, in these experiments, for those surfaces that support cellular attachment (e.g., thin PNIPAAm brushes, glass, degraded initiator), cells failed to detach from the surface at temperatures below the LCST.

We hypothesized that introducing nanopatterns within PNIPAAm would facilitate the attachment and growth of cells on thicker PNIPAAm nanopatterned brushes, while maintaining the capacity to release cells when rinsed at temperatures below the LCST of PNIPAAm. Because nanopatterned PNIPAAm/FN surfaces have not been investigated for mammalian cell culture, we first evaluated the ability of a representative nanopatterned surface (period = 274 ± 14 nm and with corresponding $t_{PNIPAAm}$ = 78.8 ± 3.5 nm,) to support the culture of NIH-3T3 fibroblast cells. **Figure 3**a–d show that the nanopatterned surfaces readily supported the attachment and the proliferation of fibroblasts, with cellular density increasing over a 72 h period until the cells reached confluence. Under these growth conditions, the majority of cells remained viable (SI, Figure S5) and exhibited a typical elongated, spread morphology as shown by scanning electron microscopy (SEM) images (SI, Figure S6). In addition to fibroblasts, nanopatterned PNIPAAm/FN surfaces also supported the growth of bovine aortic endothelial cells (SI, Figure S7), suggesting that these surfaces are suitable for culturing various mammalian cell types.

Interestingly, the inclusion of nanopatterns within the PNIPAAm enabled cells to adhere and proliferate on brushes

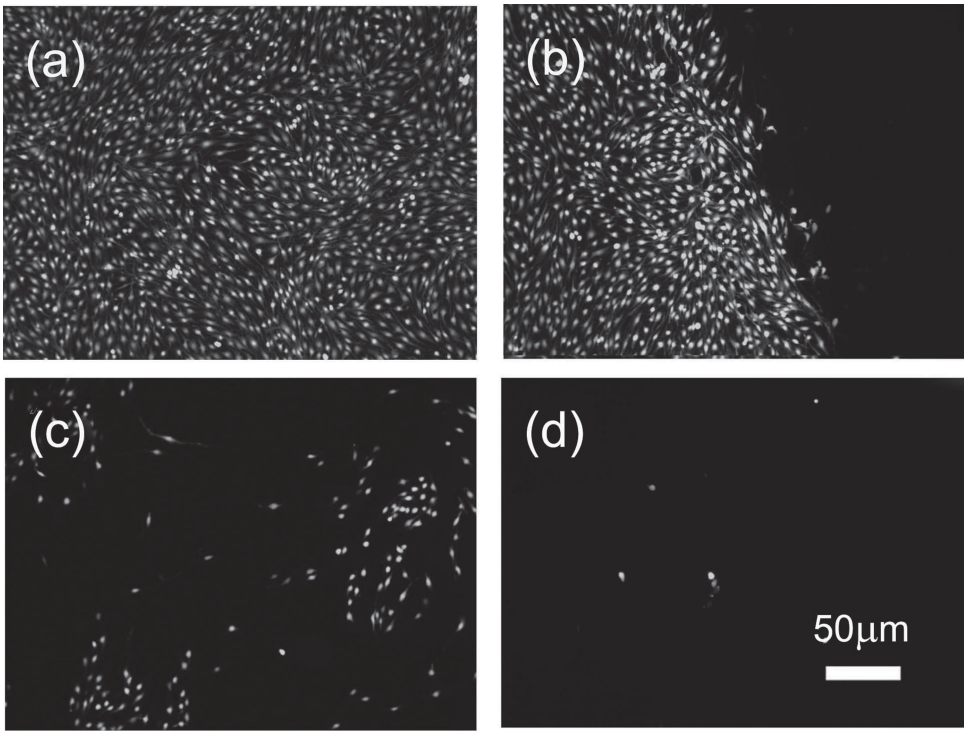

Figure 4. Representative images of NIH-3T3 fibroblasts on (a) a nanopatterned PNIPAAm/FN surface (period = 274 ± 14 nm, $t_{PNIPAAm}$ = 78.5 ± 3.5 nm), (b) the boundary area between nanopatterned/FN and unpatterned PNIPAAm/FN surface after 72 h in culture at 37 °C. (c,d) Representative images of fibroblasts remaining on a nanopatterned PNIPAAm/FN surface after incubation in buffer at 25 °C for (c) 30 min and (d) 60 min.

produced with longer polymerization times (e.g., corresponding to $t_{PNIPAAm}$ = 78.8 ± 3.5 nm), eliminating the need to maintain a narrow threshold of PNIPAAm thickness.[16–19] After 72 h, fibroblasts remained viable on nanopatterned PNIPAAm brushes. By comparison, the unpatterned PNIPAAm brushes produced using the same polymerization times (to yield $t_{PNIPAAm}$ = 78.8 ± 3.5 nm) failed to support cellular growth (**Figure 4**a,b). A distinct boundary formed between surface locations containing nanopatterned PNIPAAm (with cells) and unpatterned PNIPAAm (without cells) (Figure 4b). After reducing the temperature below the LCST, cells readily detached from nanopatterned PNIPAAm (Figure 4c,d), which demonstrates that the nanopatterned topology does not hinder the temperature triggered cellular release.

The capacity for cells to attach and proliferate on these nanopatterned PNIPAAm surfaces depends on the presence of a surface-presenting biological cue. Prior to seeding the cells, surfaces were incubated with FN at 37 °C to enhance the cellular attachment. Attempts to culture cells without FN pre-adsorption were unsuccessful. For instance, NIH-3T3 fibroblasts cultured on nanopatterned PNIPAAm surfaces without FN pre-adsorption resulted in fibroblasts with a rounded morphology, poor cellular adhesion, and low cellular densities (Figure S8). Moreover, differences in cell density existed between surfaces pre-treated with FN at 25 °C (230 ± 26 cells/mm^2) and at 37 °C (690 ± 30 cells/mm^2) (Figure S8). This further suggests that surfaces pre-treated with FN at 37 °C adsorb a higher concentration of FN, likely due to the collapse of PNIPAAm chains and exposure of the underlying substrate (Figure 2).

To assess the residual FN remaining on the surfaces after cellular detachment, we reseeded cells on the nanopatterned PNIPAAm/FN surfaces immediately after cellular removal (without re-adsorption of FN). As shown in Figure S9, fibroblasts readily attached and proliferated on these recycled surfaces, suggesting that cellular detachment does not deplete all biological cues on the surface. We further evaluated residual FN on surfaces using an immunoassay (Figure S10), which shows a significant quantity of FN on the surface after cellular detachment. However, the origin of the FN (i.e., whether from surface pre-adsorption, cellular secretion, or non-specific adsorption) was not discernible. Overall, the results presented in this section demonstrate that nanopatterned PNIPAAm serves as a biocompatible, temperature-triggered platform for the selective attachment and detachment of mammalian cells.

2.4. Cellular Response to Features of Nanopatterned PNIPAAm/FN Surfaces

We next evaluated the response of cells to two key features of nanopatterned PNIPAAm topology: the polymerization time and the period of patterns of PNIPAAm.[30] First, to evaluate the effect of polymerization time on cellular response, cells were cultured on nanopatterned PNIPAAm/FN surfaces comprising a fixed period (i.e., 274 ± 14 nm), but for samples prepared using different polymerization times. **Figure 5** shows that, at 37 °C, cells readily attached to, and proliferated on, nanopatterned surfaces with polymerization time from 1 min to 6 min (corresponding to $t_{PNIPAAm}$ from 13.0 ± 1.7 nm to 78.8 ± 3.5 nm). Irrespective of the polymerization time, the density of cells reached approximately 800 cells/mm^2 after 72 h. Although cellular attachment

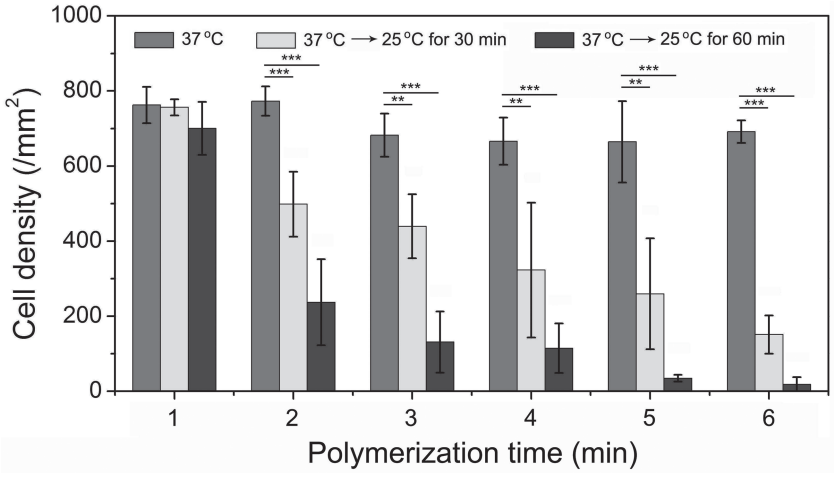

Figure 5. Number of viable, attached NIH-3T3 fibroblasts on nanopatterned PNIPAAm surfaces with a fixed period of 274 ± 14 nm and polymerization time ranging from 1 min to 6 min (corresponding $t_{PNIPAAm}$ ranging from 13.0 nm to 78.8 nm). Cells were cultured at 37 °C for 72 h prior to determining cell density, which was evaluated immediately after removal from culture conditions and after incubation in buffer at 25 °C for 30 min and 60 min. Error bars represent the standard deviation of the mean (n = 6, * $p < 0.05$, ** $p < 0.01$, *** $p < 0.001$).

and proliferation was unaffected by the polymerization time, the detachment of cells was greatly affected by this parameter. After incubation in buffer at 25 °C, cells failed to detach from surfaces prepared at shorter polymerization times (e.g., 1 min, $t_{PNIPAAm}$ = 13.0 ± 1.7 nm), whereas cell readily detached from surfaces with prepared with longer polymerization times. For the longest polymerization time (6 min, $t_{PNIPAAm}$ = 78.8 ± 3.5 nm), more than 95% of cells detached after incubation in buffer at 25 °C for 60 min.

Second, to evaluate the cellular response to the period of nanopatterns, cells were cultured on nanopatterned surfaces prepared with the same PNIPAAm polymerization time, but with different spatial periods. Specifically, a series of nanopatterned surfaces was prepared, in which the polymerization time (short: 1 min ($t_{PNIPAAm}$ = 13.0 ± 1.7 nm); medium: 3 min ($t_{PNIPAAm}$ = 46.3 ± 2.1 nm); or long: 6 min ($t_{PNIPAAm}$ = 78.8 ± 3.5 nm)) and period size (from 157 ± 9 nm to 1021 ± 17 nm) were systematically varied. **Figure 6**a–c shows that cellular detachment is significantly influenced by the polymerization time, but is unaffected by the period size over the range of periods examined. Cells detached minimally from surfaces with short polymerization times (<20% release ratio), whereas cells released extensively from surfaces with medium and long polymerization times (Figure 6d), irrespective of the period.

The studies in this section reveal two important concepts: (i) cells are relatively insensitive to the period size as compared with the polymer polymerization time (and thus, presumably, the polymer chain length), and (ii) the release ratio of attached cells increases with an increasing polymerization time. Thus, our results show that the cells do not recognize the differences in the period of nanopatterns, which ranged from 157 ± 9 nm

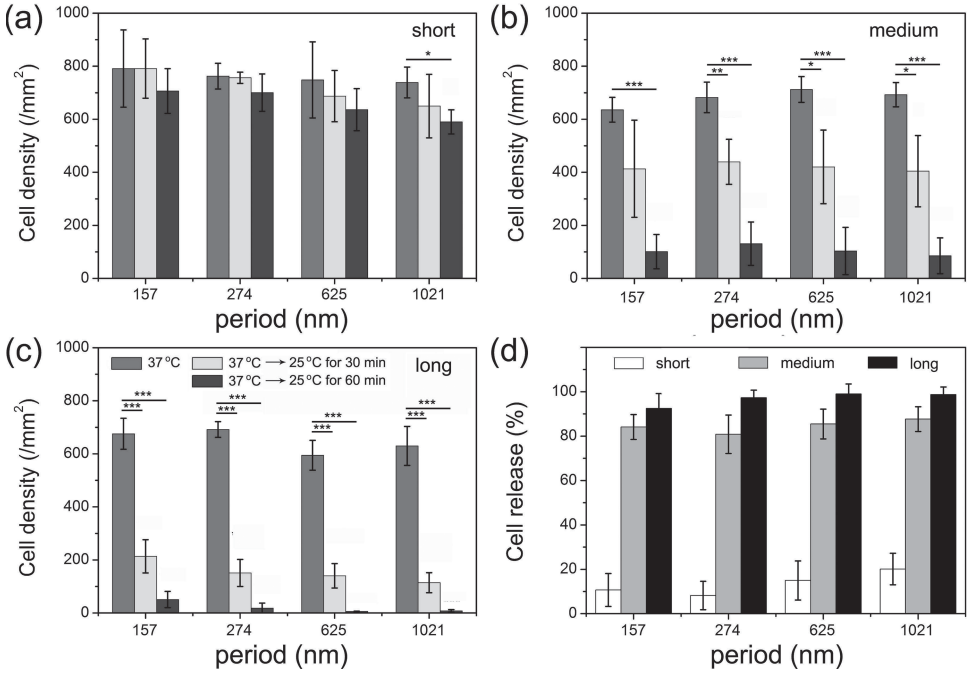

Figure 6. (a-c) Number of viable, attached NIH-3T3 fibroblasts on nanopatterned PNIPAAm surfaces with different periods for (a) short polymerization time (1 min, $t_{PNIPAAm}$ = 13.0 ± 1.7 nm), (b) medium polymerization time (3 min, $t_{PNIPAAm}$ = 46.3 ± 2.1 nm), and (c) long polymerization time (6 min, $t_{PNIPAAm}$ = 78.8 ± 3.5 nm). Cells were cultured at 37 °C for 72 h prior to determining cell density before release (red bars), and cellular detachment after removal from culture by incubation in buffer at 25 °C for 30 min (cyan bars) and 60 min (blue bars). The corresponding release ratio of 60 min is shown in (d). Error bars represent the standard deviation of the mean (n = 6, * $p < 0.05$, ** $p < 0.01$, *** $p < 0.001$).

to 1,021 ± 17 nm (for $t_{PNIPAAm}$ at 13.0 ± 1.7 nm, 46.3 ± 2.1 nm, and 78.8 ± 3.5 nm). For these surfaces, the fibroblasts did not exhibit any observable changes in growth or morphology after 72 h in culture. This result was unexpected, as several reports demonstrate that cells respond to nanoscale surface features by changing their adhesion, spreading, and proliferation.[42–46] Additional studies would be required to further understand the potential effects of period and thickness of nanopatterned PNIPAAm on other cellular responses commonly affected by nanopatterns, such as gene expression and cellular differentiation.[46]

Our results also show that the polymerization time (and likely the chain length of PNIPAAm) does not affect cellular attachment, but greatly influences cellular detachment at temperatures below the LCST. The dependence of cell detachment on the polymerization time (and thus chain length) is associated with conformational changes of PNIPAAm chains. For uniform (unpatterned) PNIPAAm brushes, self-consistent-field (SCF) calculations predict that the extent of temperature-induced conformational change of end-grafted PNIPAAm brushes increases as a function of molecular weight,[47] in qualitative agreement with results obtained from neutron reflectivity measurements.[48,49] The extent of conformation changes of PNIPAAm chains dictates cellular release.[50,51] For shorter PNIPAAm chains, the molecular mobility and hydration are significantly weakened due to the influence of substrate. The extension of PNIPAAm is likely restricted so that swollen chains are not long enough to interfere with the cell-substrate interface, resulting in limited cell detachment. Conversely, longer PNIPAAm chains have a higher degree of mobility and hydration, which likely leads to the greater cell detachment.

2.5. Micropatterning of Cells

The results in Figure 4 show that thicker unpatterned PNIPAAm/FN surfaces ($t_{PNIPAAm}$ = 78.8 ± 3.5 nm) prevent cellular attachment, whereas the corresponding nanopatterned PNIPAAm/FN surfaces support cellular attachment and proliferation. The capacity to dictate the location of cell growth based on the spatial distribution of nanopatterned brushes encouraged further investigation into micropatterning of cells. To this end, a surface comprising a grid of both micro- and nanopatterned PNIPAAm brushes on the same sample was prepared (SI, Scheme S1b). Here, the striped micro-scale areas contain unpatterned PNIPAAm, whereas the square micro-scale areas contain nanopatterned PNIPAAm. Fibroblasts exclusively attached to regions containing nanopatterned PNIPAAm, resulting in micropatterns of cells after 72 h in culture (**Figure 7**).

The ability to guide the location of cell growth based on the spatial distribution of nanopatterned brushes enabled the preparation of micropatterned cellular surfaces, which holds potential value for applications including co-culture of cells and microchip-based bioassays.[52,53] For example, this micropatterning approach holds promise for the development of high-throughput cellular biosensing assays, wherein patterned patches of cells remain isolated in predetermined locales, screened against unique variables, and mildly recovered for downstream cellular analysis. Importantly, the ability to mildly recover micropatterned cells for analysis after these applications (e.g., cell-to-cell communication studies or bioassays) would eliminate potential interferences resulting from traditional cellular release processes, such as those that use proteases. For example, studies have shown that low-temperature liftoff of cells from PNIPAAm are less damaging to both the cells and ECM, as compared to enzymatic digestion.[4] Here, the ability to mildly collect and analyze cells from predetermined micropatterned locales would be advantageous for understanding further the cellular biochemistry from a minimally disturbed state, as compared to conventional cell harvesting approaches.

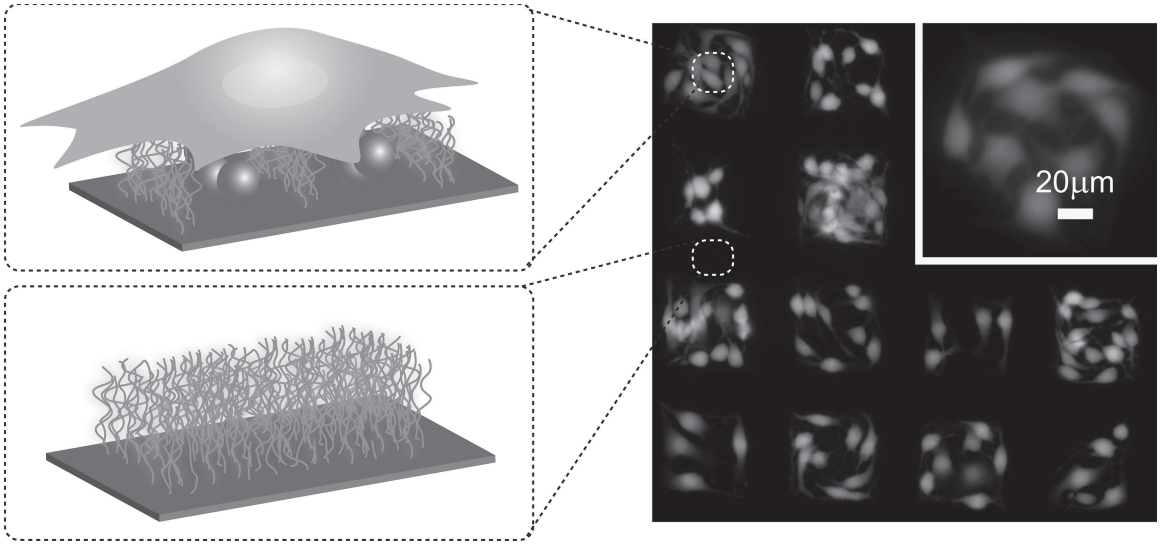

Figure 7. Patterned PNIPAAm surfaces containing both micro- and nanopatterns on the same sample (i.e., square areas contain nanopatterned PNIPAAm (period = 274 ± 14 nm, $t_{PNIPAAm}$ = 78.8 ± 3.5 nm); stripe areas contain unpatterned PNIPAAm).The representative fluorescence image shows viable NIH-3T3 fibroblasts located exclusively on the nanopatterned regions after 72 h. Cells were treated with LIVE/DEAD stain prior to imaging.

3. Conclusion

Surfaces modified with thermo-responsive PNIPAAm are advantageous for the mild harvesting of anchorage dependent cells. In this study, nanopatterns were introduced into PNIPAAm surfaces and used to culture and harvest mammalian cells, such as fibroblasts and endothelial cells. Surfaces were prepared via the combination of UV-IL and ARGET-ATRP, which permitted the rapid production of large surface areas containing nanopatterns. The pattern period size of grafted PNIPAAm was adjusted by simply changing interference angle. Above the LCST, the nanopatterned PNIPAAm chains collapse and expose the underlying substrate, facilitating the adsorption of FN onto the polymer-free intervals. The exposure of FN at 37 °C supported the attachment and proliferation of cells on surface containing nanopatterned PNIPAAm brushes with thicknesses between 13.0 ± 1.7 nm to 78.8 ± 3.5 nm. The extent of cellular detachment below the LCST at 25 °C depends on the chain length of the grafted polymer chains. Irrespective of period size, cells readily detached from nanopatterned PNIPAAm at brush thicknesses >13 nm.

This study not only explores the parameters that influence the interaction of mammalian cells with nanopatterned PNIPAAm brushes, but also demonstrates a new strategy to design well defined engineered surfaces for harvesting cells. By introducing nanopatterns within the grafted PNIPAAm brushes, we circumvented the requirement to maintain a narrow range of PNIPAAm thickness (i.e., critical thickness). Moreover, the selective attachment of cells to the nanopatterns facilitated a new approach for preparing cellular micropatterns, which holds the potential for studying the interactions of different cell types and preparing unique cell sheet sizes for tissue engineering applications. Overall, nanopatterned PNIPAAm surfaces provide a unique solution to the critical thickness issue for cell harvesting and facilitate spatial control of cellular growth and harvesting on surfaces.

4. Experimental Section

Materials: *N*-isopropylacrylamide (NIPAAm), $CuBr_2$ (98% pure), 1,1,4,7,7-pentamethyldiethylenetriamine (PMDETA, 99% pure), and ascorbic acid (reagent grade, 20–200 mesh) were purchased from Sigma-Aldrich (St. Louis, MO). The monomer was recrystallized twice from a benzene/hexane mixture and then dried under vacuum before use. The ATRP initiator (3-trimethoxysilyl) propyl 2-bromo 2-methylpropionate was purchased from Gelest (Morrisville, PA) and stored under dry conditions until use. Silicon wafers and coverslips (size = 25 × 50 mm, thickness = 0.13 mm) were purchased from University Wafer and VWR, respectively. NIH-3T3 fibroblast cells were obtained from Duke University Cell Culture Facility. Bovine aortic endothelial cells (BAECs), BAEC growth medium, and BAEC subculture reagent kit were obtained from Genlantis. The Live/Dead® viability kit, Dulbecco's modified eagle medium (DMEM), bovine plasma fibronectin (FN), penicillin-streptomycin, Fungizone® antimycotic, phosphate buffered saline (PBS), and 0.25% trypsin-ethylenediaminetetraacetic acid (EDTA) were acquired from Life Technologies. Calf serum, anti-fibronectin 1 polyclonal antibody (anti-FN1, produced in rabbit), and the anti-rabbit IgG polyclonal antibody containing the green fluorescent dye CF-488A (produced in donkey) were purchased from Sigma-Aldrich (St. Louis, MO). Rhodamine labeled-fibronectin from bovine plasma (rhodamine-FN) was obtained from Cytoskeleton, Inc.

Preparation of Surfaces: (i) Preparation of self-assembled monolayers (SAMs) of ATRP initiators. Silicon wafers and cover slips were cleaned with "Piranha" solution (7:3(v/v) 98% H_2SO_4 : 30% H_2O_2. *Caution: piranha solution reacts violently with organic materials and should be handled carefully!*) to remove the organic residue. The wafers were subsequently rinsed with an abundance of ultrapure water and dried under a dry nitrogen stream. The cleaned samples were immersed in 10 mL of anhydrous toluene containing the ATRP initiator-terminated silane (2 vol.%) at room temperature for 24 h to generate brominated surfaces. These surfaces were rinsed thoroughly with toluene and dried under a nitrogen flow. (ii) Photo-oxidation and patterning of SAMs. Interferometric lithography was performed using a two-beam interference system (Lloyd's mirror set-up) as reported previously.[29] Nanopatterns of ATRP initiator were fabricated by exposing ATRP initiator immobilized SAMs to a diode-pumped, frequency-doubled Nd: vanadate laser (Coherent, Verdi-V5) with a wavelength (λ) of 266 nm (energy dose of 13.9 J/cm^2). The pattern period was adjusted by changing the interference angle (θ) based on the equation: period = $\lambda/[2\sin(\theta/2)]$. (iii) Preparation of nanopatterned PNIPAAm surfaces. PNIPAAm polymer brushes were grafted from patterned SAMs of ATRP initiators using ARGET-ATRP.[32] Briefly, samples were immersed into a solution containing 14 mL methanol, 14 mL H_2O, 2.5 g NIPAAm, 3.15 mg $CuBr_2$, 34.5 mg ascorbic acid and 19.6 μL PMDETA. After a desired time, the samples were removed from the solution, rinsed with an abundance of ultrapure water and methanol successively to remove both unreacted NIPAAm monomer and ungrafted PNIPAAm, and then dried under a nitrogen flow. As controls, PNIPAAm brushes were also grafted from unpatterned SAMs of ATRP initiators under identical polymerization conditions.

Atomic Force Microscopy (AFM): Contact-mode topographical measurements of nanopatterned PNIPAAm surfaces in air were obtained with a Digital Instruments multimode atomic force microscope with a NanoscopeIIIa controller. The corresponding section analysis (line profile) was performed using the Nanoscope Analysis software.

Evaluating Adsorption of Fibronectin on Surfaces: Rhodamine-FN was dissolved in 1× PBS (137 mM sodium chloride, 27 mM potassium chloride, 10 mM phosphate buffer, pH 7.4) at a concentration of 0.01 mg/mL. The sample surfaces were incubated in ethanol for 20 min, rinsed three times in 1× PBS, and incubated in rhodamine-FN solution for 4 h under static conditions at either 25 °C or 37 °C. Following adsorption, the surfaces were immediately immersed in fresh protein-free PBS (three times) to remove loosely adsorbed protein. Then the surfaces were rinsed with ultrapure water quickly and dried under nitrogen stream. The adsorption of rhodamine-FN was evaluated using fluorescence microscopy (Zeiss Axioimager) with a 40× objective and a filter set comprising ex 525/25, em 605/70. All images used for comparison of fluorescence intensities were obtained using identical exposure times, image contrast, and brightness settings. Fluorescence intensity of images was analyzed using Zeiss Axio Vision software. For each sample, 10 images from random areas across the sample surface were captured and analyzed to obtain average fluorescence intensity.

Cell Culture: NIH-3T3 fibroblast cells were cultured at 37 °C, 5% CO_2 using DMEM containing 25 mM glucose supplemented with 10% calf serum, 50 U/mL penicillin, 50 μg/mL streptomycin, and 2.5 μg/mL Fungizone antimycotic. Fibroblasts were passaged using standard trypsinization methods. BAECs were cultured at 37 °C, 5% CO_2 and passaged according to protocols and reagents provided by Genlantis. Before seeding cells on samples (i.e., nanopatterned coverslips), the surfaces were sterilized in ethanol for 20 min, rinsed three times in 1X PBS, incubated with ~0.01 mg/mL bovine FN in 1X PBS for 4 h at 37 °C, 5% CO_2, and subsequently rinsed three times with 1X PBS. The 1X PBS solution for cell culture comprises 1.06 mM KH_2PO_4, 155.17 mM NaCl, 2.97 mM $Na_2HPO_4{\cdot}7H_2O$, pH = 7.4, without Ca^{2+} or Mg^{2+}. The samples were then placed inside wells (9.6 cm^2/well) within a 6-multiwell plate. Cells were seeded at 4.5 × 10^4 cells/well and cultured under standard conditions (37 °C and 5% CO_2) for a designated time (e.g., 48 or 72 h). The viability assay occurred by washing cells in 1X PBS, adding 2 mL of Live/Dead reagent to each well at 37 °C, 5% CO_2 for approximately 20 min, and subsequently rinsing the surface three times with 1X PBS.

The Live/Dead assay stains live cells green (calcein-AM) and dead cells red (ethidiumhomodimer). Fluorescent images were acquired using an upright fluorescence microscope (Zeiss Axioimager) equipped with an appropriate filter set (i.e., ex 470/40, em 525/50 for live cells and ex 545/25, em 605/70 for dead cells) and a 10X objective.

Detachment of Cells: For cell detachment, the sample surfaces were transferred to fresh 1X PBS and incubated at 25 °C for a desired period (30 min or 60 min). Then, the surfaces were gently rinsed with 1X PBS to remove the loosely attached cells. The cells remaining attached to the substrates were evaluated via fluorescence microscopy and quantified according to the number of attached cells per mm^2 as determined by ImageJ (National Institutes of Health; http://rsbweb.nih.gov/ij/; version: 1.43u). For each sample, 10 images from random areas were analyzed to obtain the average and standard deviation. Statistical analysis was performed using OriginPro 8.0 software. Statistical comparisons were made by one-way analysis of variance (ANOVA, *t*-test). P values less than 0.05 were considered significant.

Supporting Information

Supporting Information is available from the Wiley Online Library or from the author.

Acknowledgements

Q. Yu and L. M. Johnson contributed equally to this work. We thank the ONR (N00014–10–1–0907), the DTRA (HDTRA1–11–1–0004), the NSF's Research Triangle MRSEC (DMR-1121107), and The Hartwell Foundation (L. M. Johnson) for support of this work.

Received: December 24, 2013
Revised: January 27, 2014
Published online: March 13, 2014

[1] N. Matsuda, T. Shimizu, M. Yamato, T. Okano, *Adv. Mater.* **2007**, *19*, 3089.
[2] Y. Kumashiro, M. Yamato, T. Okano, *Ann. Biomed. Eng.* **2010**, *38*, 1977.
[3] M. A. Cooperstein, H. E. Canavan, *Langmuir* **2010**, *26*, 7695.
[4] H. E. Canavan, X. H. Cheng, D. J. Graham, B. D. Ratner, D. G. Castner, *J. Biomed. Mater. Res., Part A* **2005**, *75*, 1.
[5] H. E. Canavan, X. H. Cheng, D. J. Graham, B. D. Ratner, D. G. Castner, *Plasma Processes Polym.* **2006**, *3*, 516.
[6] R. M. P. da Silva, J. F. Mano, R. L. Reis, *Trends Biotechnol.* **2007**, *25*, 577.
[7] Z. Tang, Y. Akiyama, T. Okano, *Polymers* **2012**, *4*, 1478.
[8] H. G. Schild, *Prog. Polym. Sci.* **1992**, *17*, 163.
[9] I. Roy, M. N. Gupta, *Chem. Biol.* **2003**, *10*, 1161.
[10] A. Kumar, A. Srivastava, I. Y. Galaev, B. Mattiasson, *Prog. Polym. Sci.* **2007**, *32*, 1205.
[11] M. A. C. Stuart, W. T. S. Huck, J. Genzer, M. Muller, C. Ober, M. Stamm, G. B. Sukhorukov, I. Szleifer, V. V. Tsukruk, M. Urban, F. Winnik, S. Zauscher, I. Luzinov, S. Minko, *Nat. Mater.* **2010**, *9*, 101.
[12] D. L. Huber, R. P. Manginell, M. A. Samara, B.-I. Kim, B. C. Bunker, *Science* **2003**, *301*, 352.
[13] T. L. Sun, G. J. Wang, L. Feng, B. Q. Liu, Y. M. Ma, L. Jiang, D. B. Zhu, *Angew. Chem. Int. Ed.* **2004**, *43*, 357.
[14] P. M. Mendes, *Chem. Soc. Rev.* **2008**, *37*, 2512.
[15] T. Okano, N. Yamada, M. Okuhara, H. Sakai, Y. Sakurai, *Biomaterials* **1995**, *16*, 297.
[16] Y. Akiyama, A. Kikuchi, M. Yamato, T. Okano, *Langmuir* **2004**, *20*, 5506.
[17] L. Li, Y. Zhu, B. Li, C. Gao, *Langmuir* **2008**, *24*, 13632.
[18] A. Mizutani, A. Kikuchi, M. Yamato, H. Kanazawa, T. Okano, *Biomaterials* **2008**, *29*, 2073.
[19] K. Fukumori, Y. Akiyama, M. Yamato, J. Kobayashi, K. Sakai, T. Okano, *Acta Biomater.* **2009**, *5*, 470.
[20] Q. Yu, Y. Zhang, H. Chen, F. Zhou, Z. Wu, H. Huang, J. L. Brash, *Langmuir* **2010**, *26*, 8582.
[21] H. Hatakeyama, A. Kikuchi, M. Yamato, T. Okano, *Biomaterials* **2005**, *26*, 5167.
[22] M. Nishi, J. Kobayashi, S. Pechmann, M. Yamato, Y. Akiyama, A. Kikuchi, K. Uchida, M. Textor, H. Yajima, T. Okano, *Biomaterials* **2007**, *28*, 5471.
[23] O. H. Kwon, A. Kikuchi, M. Yamato, T. Okano, *Biomaterials* **2003**, *24*, 1223.
[24] F. J. Xu, S. P. Zhong, L. Y. L. Yung, Y. W. Tong, E.-T. Kang, K. G. Neoh, *Biomaterials* **2006**, *27*, 1236.
[25] M. Ebara, M. Yamato, M. Hirose, T. Aoyagi, A. Kikuchi, K. Sakai, T. Okano, *Biomacromolecules* **2003**, *4*, 344.
[26] F. J. Xu, S. P. Zhong, L. Y. L. Yung, E. T. Kang, K. G. Neoh, *Biomacromolecules* **2004**, *5*, 2392.
[27] A. M. Ross, Z. Jiang, M. Bastmeyer, J. Lahann, *Small* **2012**, *8*, 336.
[28] E. K. Yim, K. W. Leong, *Nanomedicine* **2005**, *1*, 10.
[29] Q. Yu, P. Shivapooja, L. M. Johnson, G. Tizazu, G. J. Leggett, G. P. Lopez, *Nanoscale* **2013**, *5*, 3632.
[30] Q. Yu, J. Cho, P. Shivapooja, L. K. Ista, G. P. Lopez, *ACS Appl. Mater. Interfaces* **2013**, *5*, 9295.
[31] K. Matyjaszewski, H. Dong, W. Jakubowski, J. Pietrasik, A. Kusumo, *Langmuir* **2007**, *23*, 4528.
[32] P. Shivapooja, L. K. Ista, H. E. Canavan, G. P. Lopez, *Biointerphases* **2012**, *7*, 32.
[33] D. Xia, Z. Ku, S. C. Lee, S. R. Brueck, *Adv. Mater.* **2011**, *23*, 147.
[34] M. Patra, P. Linse, *Nano Lett.* **2006**, *6*, 133.
[35] W. K. Lee, M. Patra, P. Linse, S. Zauscher, *Small* **2007**, *3*, 63.
[36] G. Tizazu, O. El-Zubir, S. R. Brueck, D. G. Lidzey, G. J. Leggett, G. P. Lopez, *Nanoscale* **2011**, *3*, 2511.
[37] M. Kaholek, W. K. Lee, B. LaMattina, K. C. Caster, S. Zauscher, *Nano Lett.* **2004**, *4*, 373.
[38] A. M. Jonas, Z. Hu, K. Glinel, W. T. S. Huck, *Macromolecules* **2008**, *41*, 6859.
[39] T. A. Horbett, *Colloids Surf., B* **1994**, *2*, 225.
[40] C. J. Wilson, R. E. Clegg, D. I. Leavesley, M. J. Pearcy, *Tissue Eng.* **2005**, *11*, 1.
[41] Q. Yu, Y. Zhang, H. Chen, Z. Wu, H. Huang, C. Cheng, *Colloids Surf., B* **2010**, *76*, 468.
[42] G. Maheshwari, G. Brown, D. A. Lauffenburger, A. Wells, L. G. Griffith, *J. Cell Sci.* **2000**, *113*, 1677.
[43] A. S. G. Curtis, B. Casey, J. O. Gallagher, D. Pasqui, M. A. Wood, C. D. W. Wilkinson, *Biophys. Chem.* **2001**, *94*, 275.
[44] M. J. Dalby, S. Childs, M. O. Riehle, H. J. H. Johnstone, S. Affrossman, A. S. G. Curtis, *Biomaterials* **2003**, *24*, 927.
[45] M. Arnold, E. A. Cavalcanti-Adam, R. Glass, J. Blümmel, W. Eck, M. Kantlehner, H. Kessler, J. P. Spatz, *ChemPhysChem* **2004**, *5*, 383.
[46] J. Y. Lim, H. J. Donahue, *Tissue Eng.* **2007**, *13*, 1879.
[47] S. Mendez, B. P. Andrzejewski, H. E. Canavan, D. J. Keller, J. D. McCoy, G. P. Lopez, J. G. Curro, *Langmuir* **2009**,
[48] H. Yim, M. S. Kent, S. Satija, S. Mendez, S. S. Balamurugan, S. Balamurugan, G. P. Lopez, *J. Polym. Sci. Part B: Polym. Phys.* **2004**, *42*, 3302.
[49] H. Yim, M. S. Kent, S. Mendez, G. P. Lopez, S. Satija, Y. Seo, *Macromolecules* **2006**, *39*, 3420.
[50] H. Takahashi, M. Nakayama, M. Yamato, T. Okano, *Biomacromolecules* **2010**, *11*, 1991.
[51] K. Nagase, M. Watanabe, A. Kikuchi, M. Yamato, T. Okano, *Macromol. Biosci.* **2011**, *11*, 400.
[52] D. G. Anderson, S. Levenberg, R. Langer, *Nat. Biotechnol.* **2004**, *22*, 863.
[53] Y. Tsuda, A. Kikuchi, M. Yamato, A. Nakao, Y. Sakurai, M. Umezu, T. Okano, *Biomaterials* **2005**, *26*, 1885.